Terrestrial responses of low-latitude Asia to the Eocene-Oligocene climate transition revealed by integrated chronostratigraphy

Yong-Xiang Li[1], Wenjun Jiao[1], Zhonghui Liu[2], Jianhua Jin[3], Dehai Wang[4], Yuxin He[5], and Cheng Quan[6]

[1] State Key Laboratory for Mineral Deposits Research, School of Earth Sciences and Engineering, Institute of Geophysics and Geodynamics, Nanjing University, Nanjing 210046, China

[2] Department of Earth Sciences, The University of Hong Kong, Hong Kong, China

[3] State Key Laboratory of Biocontrol and Guangdong Key Laboratory of Plant Resources, School of Life Sciences, Sun Yat-sen University, Guangzhou 510275, China

[4] College of Earth Sciences, Jilin University, Changchun 130061, China

[5] Department of Earth Sciences, Zhejiang University, Hangzhou, China

[6] Research Center of Paleontology and Stratigraphy, Jilin University, Changchun 130026, China

Correspondence to: Yong-Xiang Li (yxli@nju.edu.cn); Cheng Quan (quan@jlu.edu.cn)

Abstract

The Paleogene sedimentary records from southern China hold important clues to the impacts of the Cenozoic climate changes on low-latitudes. However, although there are extensive Paleogene terrestrial archives and some contain abundant fossils in this region, few are accurately dated and have a temporal resolution adequate to decipher climate changes. Here we present a detailed stratigraphic and paleomagnetic study of a fossiliferous late Paleogene succession in the Maoming Basin, Guangdong Province. The succession consists of oil shale of the Youganwo Formation (Fm) in the lower part and the overlying sandstone-dominated Huangniuling Fm in the upper part. Fossil records indicate that the age of the succession

possibly spans from late Eocene to Oligocene. Both the Youganwo Fm and the overlying Huangniuling Fm exhibit striking sedimentary rhythms, and spectral analysis of the depth series of magnetic susceptibility of the Youganwo Fm reveals dominant sedimentary cycles at orbital frequency bands. The transition from the Youganwo oil shale to the overlying Huangniuling sandstones is conformable and represents a major depositional environmental change from a lacustrine to a deltaic environment. Integrating the magnetostratiphic, lithologic, and fossil data allows establishing a substantially refined chronostratigraphic framework that places the major depositional environmental change at 33.88 Ma, coinciding with the Eocene–Oligocene climate transition (EOT) at ~33.7 to ~33.9 Ma. We suggest that the transition from a lacustrine to deltaic environment in Maoming Basin represents terrestrial responses to the EOT and indicates prevailing drying conditions in low-latitude regions during the global cooling at EOT.

1 Introduction

The Late Paleogene witnessed one of the most prominent climatic changes in the Cenozoic, a transition from greenhouse to icehouse world. The transition is climaxed at the Eocene–Oligocene boundary when marine sediments registered a large, widespread, and rapid cooling in oceans (e.g., Zachos et al., 2001; Liu et al., 2009; Bohaty et al., 2012), which was accompanied by a sudden deepening of the carbonate compensation depth (CCD) by ~1.2 km (Pälike et al., 2012) in oceans and a severe calamity in the marine community that gave rise to the largest marine mass extinction since the end of Cretaceous (e.g., Prothero, 1994; Pearson et al., 2008; Cotton and Pearson, 2011). On land, this transition is expressed as rapid ice sheet growth over Antarctic (e.g., DeConto and Pollard, 2003; Coxall et al., 2005; Goldner et al., 2014) and large-scale cooling (e.g., Zanazzi et al., 2007; Dupont-Nivet et al., 2007; Hren et al., 2013). While the transition is widely recognized in the marine realm (Zachos et al., 2001; Jovane et al., 2006; Liu et al., 2009; Pälike et al., 2012; Westerhold et al., 2014) and is increasingly well-defined in terrestrial records from the Atlantic region (e.g., Zanazzi et al., 2007; Hren et al., 2013), its impacts on Asian environment remain poorly understood. This is largely because the concomitant tectonism, i.e., the Tibetan plateau uplift, and the development of monsoonal climate may also impose strong influence on Asian environment (e.g., Dupont-Nivet et al., 2007; Quan et al., 2012, 2014; Wang et al., 2013; Licht et al., 2014, 2015; Shukla et al., 2014).

There are numerous basins in southern China that host conspicuous Cenozoic sedimentary archives documenting the Cenozoic climate changes in the region. The late Paleogene sedimentary records from this region are of particular interest because they hold clues to the dramatic shift of climates in low-latitude Asia (Quan et al. 2012; Wang et al., 2013; Licht et al., 2014, 2015), where the influence of the Tibetan Plateau uplift should be minimal in comparison to the Asian interior. However, although abundant Paleogene sedimentary successions were developed here (e.g., Tong et al., 2005; 2013), their age controls are generally poor. Despite the fact that some successions contain vertebrate and/or plant fossils (e.g., Tong et al., 2005; 2013), the indicative age ranges of these fossils are often too broad to date climate changes with satisfactory accuracy and precision.

In this paper, we present a detailed stratigraphic and paleomagnetic study on the fossiliferous Eocene to Oligocene succession in the Maoming Basin of Guangdong Province, southern China to construct a new chronostratigraphic framework that is based on an integrated litho-, bio-, magneto-, and cyclostratigraphy. The new chronology not only greatly reduces the uncertainty but also significantly refines the available fossil-based timescale of the succession. In particular, the substantially refined chronology permits establishing the link between the dramatic environmental change in the basin and the global Eocene-Oligocene climatic transition, and thus provides a critical chronological basis for further detailed examination of climate changes in this region.

2 Geologic setting

The Maoming Basin is an intramontane basin situated in the southwestern part of Guangdong Province, southern China (Fig. 1). The Cenozoic succession of the basin consists of, from the bottom to the top, the Shangdong Formation (Fm), Youganwo Fm, Huangniuling Fm, Shangcun Fm, Laohuling Fm, and Gaopengling Fm (BGMRGP, 1988, 1996). Among these units, the Eocene to Oligocene strata concern the Youganwo Fm and the Huangniuling Fm (Fig. 2).

The Youganwo Fm is characterized by the occurrence of siltstones and shales containing coal seams in the lower part and the predominant occurrence of oil shales in the upper part (Fig. 2). The Youganwo Fm contains abundant vertebrate and plant fossils including turtles of *Anosteira maomingensis, Isometremys lacuna* and *Adocus inexpectatus* (Chow and Liu, 1955; Chow and Yeh, 1962; Claude et al., 2012; Danilov et al., 2013), crocodiles of *Tomistoma petrolica* and Alligatoridae (Yeh, 1958; Li, 1975; Skutschas et al., 2014), fish of *Cyprinus*

maomingensis (Liu, 1957), mammals of *Lunania* cf. *L. youngi* (Wang et al., 2007), and wood of *Bischofia maomingensis* and *Myrtineoxylon maomingensis* (Feng et al., 2012; Oskolski et al., 2013). The age of the formation is controversial, varying from Eocene to Oligocene (e.g., Liu, 1957; Yeh, 1958; Yu and Wu, 1983). A comprehensive review of the fossil records suggests that the Youganwo Fm was most likely deposited in the late Eocene (Jin, 2008). The late Eocene age is interpreted to include both Priabonian stage and the Bartonian stage of the Eocene based on recent advances in understanding fossil mammals of *Lunania*. Although the systematic position of the genus *Lunania* is still not fully understood, increasing evidence appears to point its age at Bartonian to Priabonian stage of the Eocene. To date, two species in total were reported: *Lunania zhoui* from the Yuanqu Basin of central China (Huang, 2002), and *Lunania youngi* from Yunnan (Chow, 1957; Zong et al., 1996) and Maoming (Wang et al., 2007) of southern China, respectively. The geological age of *Lunania zhoui* is regarded to be no earlier than Bartonian and no later than Priabonian (Tong et al., 2005). For the *Lunania youngi* from Yunnan, its age spans from the Bartonian to Priabonian (Li and Ting, 1983; Russell and Zhai, 1987; Wang, 1992; Qiu and Wang, 2007), the Bartonian (Tong et al., 1995), the early Late Eocene (Huang and Qi, 1982), or the latest Eocene (Tong et al., 2005; Wang, 1997). Therefore, the late Eocene age of the mammal fossil in Maoming Basin should be understood as including both the Priabonian stage and the Bartonian stage of the Eocene.

The overlying Huangniuling Fm consists mainly of sandstones and siltstones (Fig. 2). The lower part of the Huangniuling Fm is dominated by massive, pebbly coarse sandstones interbedded with thinly bedded, grey, silty mudstones. This formation contains plenty of plant macrofossils such as fruits, leaves and reproductive remnants (e.g., Feng et al., 2013). The age of the Huangniuling Fm has been ascribed to late Eocene to Oligocene, or even to the Miocene (Yu and Wu, 1983; Wang et al., 1994; Guo, 2006; Aleksandrova et al., 2012).

The areal extent of these two formations and other Cenozoic architectural units in the Maoming Basin was mapped by Guo (2006) that compiled stratigraphic data from drill cores and outcrops. Sedimentary facies analyses of these sedimentary units indicate that alluvial fan and fan delta were initially developed in the north-eastern part of the basin, which gradually gave rise to lacustrine environment that expanded to the whole basin and alternated with deltaic environment as lake area waxed and waned (Guo, 2006). Accordingly, successions that were accumulated in the lacustrine and deltaic environments often exhibit various subfacies and microfacies. For instance, subfacies/microfacies analysis indicates that the

lower part of the Youganwo Fm was initially formed in a littoral zone to shallow lake environment that was replaced by a prodelta environment and subsequently by a shallow lake environment (Guo, 2006). The oil shale dominated upper part of the Youganwo Fm was deposited mainly in semi-deep or deep lake environments that gave rise to a shallow lake environment at the uppermost of the Youganwo Fm. The Huangniuling Fm was deposited predominately in deltaic environments that vary from prodelta, delta front to delta plain environments (Guo, 2006). The uppermost part of the Huangniuling Fm, which consists of mainly muddy siltstone and mudstones, was deposited in a prodelta environment that transitioned to a shallow lake environment where the younger Shangcun Fm was deposited.

A magnetostratigraphic study was previously conducted in the Maoming Basin (Wang et al., 1994). The paleomagetic data were collected from three different sites, drill cores MR and MB as well as an outcrop section MS (Fig. 1b), and stratigraphic data from these three sites were compiled to obtain a composite stratigraphy that comprises the upper part of Youganwo Fm, Huangniuling Fm, Shangcun Fm, and Laohuling Fm.. The age of the composite stratigraphy was interpreted to span from Chron 18n to Chron 12n (Wang et al., 1994). However, the magnetostratigraphy of Wang et al (1994) can only be regarded as preliminary by modern standards because of the following reasons. The mean sampling spacing is large, ~2.6 m; In addition, changes in sedimentation rates as indirectly reflected by the lithology were not taken into account. Furthermore, despite that samples of the Huangniuling Fm, Shangcun Fm, and Laohuling Fm were collected from the same core, i.e., the 874 m long MR core, samples of the Youganwo Fm were collected from both the MB core (15 samples) and the MS section (17 samples). The MB core is 567 m long, penetrates the Cenozoic strata, and reaches the Cretaceous rocks. No details were available as to how these 32 samples from two different sites were integrated to make a composite stratigraphy for the Youganwo Fm, particularly given that the MB core is relatively condensed and its base reaches the Cretaceous rocks. In particular, concerning the stratigraphic interval equivalent to that of this study, i.e., the upper Yougnawo Fm and the lower Huangniuling Fm, the sampling spacing was on average about 6.0 m (Figs 2 and 5 of Wang et al., 1994), which is too large by modern standards.

3 Methods

The study section is well exposed in the cliffs of the now-abandoned open mine pit (N21° 42.3', E110° 53.9'), located to the northwest of the Maoming City (Fig. 1). The exposed

section comprises the upper part of the Youganwo Fm and the overlying Huangniuling Fm. To detect subtle changes in lithology of the exposed Youganwo Fm, magnetic susceptibility (MS) was measured with a hand-held susceptibility meter SM30, typically at every 10 to 20 cm. Spectral analysis of the depth MS data series was performed using the technique of Muller and MacDonald (2000) to detect the dominant sedimentary cycles. For the overlying Huangniuling Fm, it is basal 30 meter was measured and major lithological changes in its upper part are noted.

Oriented paleomagnetic samples were collected from the exposed Youganwo Fm and the lower part of the overlying Huangniuling Fm at a depositional center of the basin where the gradual transition between the two formations occur (see Section 4.1). For oil shales in the Youganwo Fm, samples were collected usually every ~30 to 40 cm and, where possible, 2 core samples were taken from a stratigraphic level. For the Huangniuling Fm, samples were mainly collected from the interbedded thin, gray mudstones. A gasoline-powered portable rock drill was used to collect samples and a Pomery orientation device was used to orient the samples. Oriented block samples were taken from outcrops where drilling is not possible. A total of 109 core samples and 66 block samples from 122 stratigraphic levels were collected from this section.

In the laboratory, the samples were trimmed to standard cylindrical paleomagnetic specimens or cut into 2cm × 2cm × 2cm cubes. Anisotropy of magnetic susceptibility (AMS) of all specimens was measured with a KLY-3 Kappabridge. The specimens were then subjected to progressive thermal or AF (alternating field) demagnetization. The AF demagnetization was performed with a Molspin demagnetizer and the thermal demagnetization was conducted with an ASC TD48 thermal demagnetizer. The remanence of specimens was measured with a three-axis, 2G Enterprise Inc. 755 rock magnetometer. To constrain the magnetic mineralogy, isothermal remanent magnetization (IRM) acquisition was conducted with an ASC impulse magnetizer (IM-30) for selected samples. In the IRM acquisition experiments, each sample was magnetized in a forward field that progressively increases from 20 mT to 1.2 T. The sample was then progressively demagnetized in a backward field to estimate the coercivity of magnetic minerals. Between each magnetization/demagnetization treatment, the remanece of the sample was measured with an AGICO JR6A magnetometer. In addition, selected samples were subjected to a Lowrie test (Lowrie, 1990) to further constrain the magnetic mineralogy. In the Lowrie test, the samples were first magnetized sequentially along their Z, Y, and X

axes with fields of 1.2 T, 0.6 T, and 0.125 T, respectively, and the composite IRM was then thermally demagnetized up to 640 °C. To further aid in magnetic mineralogy determination, thermal changes of magnetic susceptibility of representative samples from the Youganwo Fm and the Huangniuling Fm were measured with a MFK Kappabridge equipped with CS4 apparatus. The magnetic susceptibility of the samples was measured while the samples were heated and cooled between the room temperature and 700 °C in an argon environment. In addition, Zero-field-cooled (ZFC) and field-cooled (FC) low-temperature measurements were conducted with a MPMS system at the Paleomagnetism Laboratory of Chinese Academia of Science. All the demagnetization experiments and remanence measurements were conducted in a magnetically shielded room (residual field < 300 nT) in the Paleomagnetism Laboratory of Nanjing University, China.

The demagnetization data were analyzed using the principal component analysis technique (Kirschvink, 1980). The demagnetization data are presented graphically with vector end point diagrams (Zijderveld, 1967). Software packages Puffinplot (Lurcock and Wilson, 2012) and PMGSC (by Randy Enkin) were used for paleomagnetic data analysis. The defined polarity zones, together with constraints from the paleontologic and lithologic data, are compared with the Geomagnetic Polarity Time Scale (GPTS) of Ogg (2012) to establish a chronologic framework for the investigated section.

4 Results

4.1 Sedimentary rhythms

The lithostratigraphy of the investigated section is summarized in Fig. 2. The lithology difference of the Youganwo Fm at the lower part and the Huangniuling Fm at the upper part of the section is indicated by the distinct color contrast (Fig. 2c-e). The overall light brownish color in the lower part characterizes the exposed Youganwo oil shale, while the overall pale grey to light yellowish color in the upper part characterizes the overlying, sandstone-dominated Huangniuling Fm (Fig. 2e). One of the most striking features of the outcrop is the occurrence of sedimentary rhythms, which are impressively expressed as the repeated occurrence of beds with distinct reddish color, in both the Youganwo Fm and the Huangniuling Fm (Fig. 2c, e). In the Youganwo Fm, there are more than a dozen of beds displaying distinct reddish color (Fig. 2a). The sedimentary rhythm is particularly well expressed between ~11 m and 30 m, where the average spacing between two neighboring

reddish beds is about 1.0 to 1.5 m (Fig. 2a). Inspection of the beds with reddish color at the outcrop found that the reddish coloration only occurs at the surface and should represent weathering banding of the beds because the fresh exposure of these beds does not show reddish color. Despite that the reddish color represents recent weathering, not the depositional signature, weathering enhanced the expression of changes in lithology and made the subtle lithological changes more distinctly and expressively visible on the outcrop. Because the reddish layers correspond to higher magnetic susceptibility (MS) values and less reddish levels display relatively lower magnetic susceptibility values, MS data can facilitate the characterization of sedimentary rhythms in the Youganwo Fm. Indeed, our high-resolution MS data also exhibit meter-scale cyclicity (Fig. 2b). Spectral analysis of the MS data reveals dominant sedimentary cycles with a cycle wavelength of ~252 cm, 127 to 107 cm, and ~30 cm (Fig. 3). The 127 to 107 cm cycle and the ~30 cm cycle have a cycle wavelength ratio of 3.6 to 4.2:1, which is similar to the periodicity ratio of 4:1 for the long eccentricity and the short eccentricity. The ~252 cm cycle and the 127 to 107 cm cycle have a cycle wavelength ratio of 1.98 to 2.35:1, probably representing the harmonics of the 127 to 107 cm cycle. Therefore, the dominant sedimentary cycles are probably in the orbital frequency bands and the meter-scale cycles may represent the long eccentricity cycle. Since the Youganwo oil shale was formed in a lacustrine environment (Guo, 2006), the subtle lithological changes in a repeated fashion as exemplified by the occurrence of the meter-scale sedimentary rhythms were probably related to fluctuating lake levels, which can cause subtle changes in deposition, thus in lithology. Fluctuations of lake level in Maoming Basin may have been modulated by orbital variations because the dominant sedimentary cycles appear to be in the orbital frequency bands.

The contact between the Youganwo Fm and the overlying Huangniuling Fm is sharp at many locations around the edge of the open mine pit where the siltstone and sandstone dominated Huangniuling Fm directly sit atop of brown grey to dark grey mudstones of the upper part of the Youganwo Fm. However, when the contact is traced toward the center of the basin, the interface between the two formations is represented by a ~ 50 cm thick layer that displays a continuous, gradual change from brown grey mudstones at the uppermost Youganwo Fm to pale grey mudstones at the base of the Huangniuling Fm (Fig. 2d). Above the pale grey mudstone are siltstones and sandstones, exhibiting a coarsening upward trend in grain size. Further upsection, the siltstones and sandstones are interbeded with thin layers of pale grey mudstones in the lower part of the Huangniuling Fm. These features suggest that the

deposition was continuous at the study site when the Maoming Basin experienced the transition from a shallow lacustrine environment, as represented by the upper part of the Youganwo Fm to a prodelta environment, as represented by the lower part of the Huangniuling Fm (Guo, 2006), while the lake level was probably dropping.

In the Huangniuling Fm, the distinct red layer consists of coarse sandstones. It occurs at the base of the pale grey massive coarse sandstone and is typically a few centimeters thick. The basal red sandstones are more resistant to weathering than the rest of the massive sandstones and commonly stick out of the surface of the outcrop, making the distinct red layers readily recognizable at distance (Fig. 2c). The thickness of the massive sandstone varies largely from decimeters to meters, occasionally up to decameters. Above massive sandstones is typically a relatively thinner mudstone bed (Fig. 2c). A red layer, massive sandstones, and a thin mudstone bed appear to form a parasequence that occurs repeatedly across the Huangniuling Fm (Fig. 2a, b, c). In the lower part of the Huangniuling Fm, the sandstone and mudstone beds in a parasequence are nearly flat and extend laterally with uniform thickness for hundreds of meters, and there is a fining-upward trend within a parasequence, suggesting that this part of the Huangniuling Fm was deposited in a prodelta to delta front or an interdistributary bay environment. Given the gradual nature of the transition from the Youganwo Fm to the Huangniuling Fm, the repeated occurrence of the parasequence in the lower part of the Huangniuling Fm was probably associated with fluctuating lake levels that may have been forced by orbital variations as well. This notion of orbital forcing is supported by the persistent pattern of rhythmic occurrence of the parasequences. This notion is also strengthened by the demonstrated orbital forcing of the deposition in marine (e.g., the Eocene/Oligocene boundary GSSP section in Italy, Jovane et al., 2006) and lacustrine (e.g., the Green River Fm, Meyers, 2008) settings during the similar time interval. In the upper part of the Huangniuling Fm, lense-shaped channelized sandstones are occasionally observed, suggesting that delta front to delta plain deposits gradually became dominant in the upper section. Using the distinct red layer in a parasequence as a marker bed, we have counted 19 parasequences, representing 19 sedimentary cycles, in the exposed Huangniuling Fm (Fig. 2a, b).

4.2 Rock magnetic data

4.2.1 Anisotropy of magnetic susceptibility (AMS)

The AMS data of the Youganwo samples show predominantly oblate fabrics with the minimum axes perpendicular to the bedding and the maximum and intermediate axes parallel or subparallel to the bedding (Fig. 4a,b). The degree of anisotropy (Pj) ranges from 1.0 to 1.232 (Fig. 4b). The AMS data of the Huangnuling samples display mainly oblate fabrics (Fig. 4d), but also show a weak prolate fabric with the maximum axes trending SE and the minimum and intermediate axes girdling along the NE-SW direction (Fig. 4c). In addition, the degree of anisotropy of the Huangniuling samples is low, varying from 1.0 to 1.089, and mostly below ~1.03 (Fig. 4d).

4.2.2 Temperature-dependence magnetic properties and IRM

Thermomagnetic curves of the samples show that all the low-field magnetic susceptibility values at the end of the experiments are higher than those at the beginning of the experiments, suggesting that transformation of magnetic mineral phases occurred during heating (Fig. 5a-e). Because the cooling curves generally show a rapid increase in susceptibility from 580°C to 500°C (Fig. 5a-e), magnetite were probably produced during the experiments, leading to elevated susceptibility values by the end of the experiments. The mudstone at the lower part of the Huangniuling Fm (Fig. 5a,b) and the brown grey shale of the uppermost Youganwo Fm (Fig. 5c) show overall similar features with an increase in magnetic susceptibility between 450°C and 500°C during heating, whereas the oil shale samples show an increase in magnetic susceptibility at ~250°C and another major increase between 400°C and 450°C (Fig. 5d,e) during heating. For the oil shale samples, the magnetic susceptibility increase at ~250°C (Fig. 5d,e) is diagnostic of hexagonal pyrrohtite due to thermally activated vacancy ordering (Dunlop and Özdemir, 1997), and the subsequent increase in magnetic susceptibility between 450°C and ~500°C probably indicates transformation of pyrrohtite to magnetite during heating (Fig. 5d,e).

IRM acquisition of the samples shows that these samples are mostly saturated at fields above 200 mT (Fig. 5f). The demagnetization of IRMs in the backward DC fields suggests that the coercivity of the magnetic minerals is around 40 mT (Fig. 5f). The ZFC and FC low-temperature data of the samples show that the Huangniuling mudstone and the brown grey shale of the uppermost part of the Youganwo Fm exhibit similar features that are

characterized by a small difference between the ZFC and FC curves (Fig. 5g, h). In addition, the Huangniuling mudstone shows a subdued transition at ca. 120 K (Fig. 5g), indicative of the presence of magnetite (Verwey, 1939; Özdemir et al., 1993). Thermal demagnetization of the composite IRM of the Huangniuling mudstone and the brown grey shale of the Youganwo Fm shows that the low coercivity component (0.125 T) unblocked at 580°C, confirming that magnetite is the major magnetic mineral phase in the Huangniuling mudstone and the brown grey shale of the uppermost of the Youganwo Fm. For the Youganwo oil shale, in addition to the presence of pyrrhotite as indicated by the rapid increase in magnetic susceptibility at ~250°C (Fig. 5d,e), magnetite is present as well, which is evidenced by the 580°C unblocking temperature of the composite IRM (Fig. 5o). At some oil shale levels such as around 17.2 m, iron suphide phases become predominant, which is indicated by the sharp drop of the composite IRM between 350°C and 400°C (Fig. 5n). ZFC and FC low-temperature measurements show that there is a marked difference between the ZFC and FC curves (Fig. 5i, j), indicating the presence of pyrrhotite (Snowball and Torii, 1999). The Mr/χ ratio of the Youganwo oil shale is typically around 0.5 x 10^3 to 1.0 x 10^3 A/m, which is low in comparison to the ~ 70 x10^3A/m for greigite (Snowball and Thompson, 1990). Also, greigite tends to display little difference between ZFC and FC curves (Chang et al., 2007; Roberts et al., 2011). Therefore, greigite may not be present in Youganwo oil shale. Pyrrhotite is the dominant iron sulphide phases in the Youganwo oil shale.

4.3 Paleomagnetic data

Natural remanent magnetizations (NRMs) of the samples range between 3 × 10^{-3} and 20 mA/m with the majority being at the orders of 10^{-2} to 10^{-1} mA/m. About half of the specimens are magnetically unstable, displaying erratic directions upon demagnetization. For the rest of the samples, the AF demagnetized samples generally show demagnetization trajectories decaying toward the origin (Fig. 6a, b, c) and the thermally demagnetized samples generally show relatively stable demagnetization trajectories below 400 °C (Fig. 6d, e, f), above which erratic directions occur. For most samples, the linear segment of the demagnetization trajectory with coercivities > 15 mT or with a temperature range from ~150 °C to ~340°C or 380°C that decays toward the origin is regarded as a characteristic remanence (ChRM). The demagnetization data together with the rock magnetic data (Section 4.2.2) suggest that the

remanence of the samples mainly resides in magnetite and pyrrhotite becomes the dominant magnetic mineral phase in the Youganwo oil shale.

To obtain reliable estimates of the ChRMs, the following criteria are also used to scrutinize the data: a) we generally accept ChRMs of higher coercivity/unblocking temperature component decaying toward the origin with at least four data points; b) ChRMs with a maximum angular deviation (MAD) greater than 16° are rejected; c) if two samples from the same stratigraphic level yield similar ChRMs, the sample that has a better definition of the ChRM is used. Following the above treatments, we obtain reliable paleomagnetic data from 63 stratigraphic levels. Among these data, ChRMs from 46 stratigraphic levels have their corresponding virtual geomagnetic pole (VGP) within 45° from the mean of VGPs. These 46 ChRMs show both normal and reversed polarities (Fig. 7). A reversal test was performed and passed at 95% confidence level with class "C" (McFadden and McElhinny, 1990). Therefore, the quality of the 46 ChRMs is ranked at "A" and the remaining 17 ChRMs are ranked at "B" in quality. Changes in inclinations and VGP latitudes of these ChRMs with depth are shown in Fig. 8c, d.

5 Discussions

5.1 Definition of magnetozones

Oil shales in the Youganwo Fm exhibit predominantly oblate AMS fabrics (Fig. 4), indicative of a depositional origin of the fabrics. Silty mudstone layers in the Huangniuling Fm also show mainly oblate AMS fabrics, and prolate fabrics occur as well, though weak. These features indicate depositional type of fabrics developed in the presence of currents flowing at a moderate speed (Tauxe, 1998), which is consistent with a deltaic depositional environment for the Huangniuling Fm. In addition, reversed polarities are present and a reversal test passed (Section 4.3). Taking together, the occurrence of depositional type fabrics, the presence of reversed polarities, and the passage of a reversal test suggest that the remanence is likely primary. Therefore, both the VGP latitudes and inclinations are used to define magnetozones of the investigated section (Fig. 8e). Also, definition of magnetozones is primarily based on the "A"-quality ChRM data and the "B"-quality ChRM data are only used as a second-order constraint for intervals where "A"-quality data are sparse (Fig. 8c, d). In addition, a polarity zone is defined by at least two consecutive levels of similar polarities. Changes in inclinations and VGP latitudes with depth are largely in concert, which allows us to define two reversed

polarity zones (R1 and R2) and two main normal polarity zones (N1 and N2) (Fig. 8e). Among these magnetozones N1 and R2 are better defined. N1 is defined between 32.2 m and 51.0 m, and R2 is defined from 25.0 m to 32.2 m (Fig. 8e). Below 25.0 m is dominated by the normal polarities except at ~ 10 m where isolated negative inclinations and VGP latitudes occur (Fig. 8c, d). Although these negative values do not occur consecutively in depth (Fig. 8c, d), the trend of shift toward negative values in both inclinations and VGP latitudes is evident and is consistent, suggesting that a reversed polarity probably exists at ~10 m (Fig. 8e). This possible reversed polarity zone is tentatively defined between ~11.0 m and ~8.5 m and separates the lower 25 m section into two short normal polarity zones, N2 and N3 (Fig. 8e).

5.2 Major constraints on a geomagnetic polarity timescale (GPTS)

Correlation of these magnetozones to the standard GPTS is not unique due to the lack of numerical ages serving as anchor points. However, several constraints exist for the investigated section. When these constraints are used collectively and in conjunction with the defined magnetozones (Fig. 8e), it is possible to establish a reliable polarity time scale for this section.

The major constraints are as follows. 1), the studied oil shales contain abundant vertebrate and plant fossils (Chow and Liu, 1955; Liu, 1957; Yeh, 1958; Chow and Yeh, 1962; Li, 1975; Yu and Wu, 1983; Wang et al., 2007; Claude et al., 2012; Feng et al., 2012, 2013). In particular, the mammal fossil (*Lunania* cf. *L. youngi*) (Wang et al., 2007), which was unearthed from the studied oil shale of the Youganwo Fm, provides the most definitive evidence for a late Eocene age (Wang et al., 2007; Jin et al., 2008). Accordingly, the Youganwo oil shale was formed sometime in the Priabonian stage and/or Bartonian stage of the Eocene that could span from magnetic Chrons C18r to C13r, i.e., 41 to 34 Ma (Fig. 8f). 2), the marked difference in lithology of the Youganwo Fm and the Huangniuling Fm suggests drastic difference in sediment accumulation rates. The sampled Youganwo Fm consists predominantly of brown oil shales, whereas the overlying Huangniuling Fm comprises dominantly massive pebbly coarse sandstones and siltstones. Therefore, the sediment accumulation rates for the Huangniuling Fm were much faster than those for the Youganwo Fm. In addition, although organic matter and silt content decreases upsection and grey mudstones occur at the uppermost of the Youganwo Fm, changes in lithology within the Youganwo Fm are subtle. This suggests that sediment accumulation rates of the studied Youganwo Fm should not

change drastically. 3), the deposition between the Youganwo and Huangniuling Fms is continuous. The contact between the two formations displays a continuous, gradual change from brown grey mudstones at the uppermost Youganwo Fm to pale grey mudstones at the base of the Huangniuling Fm within an interval of ~50 cm. In addition, siltstones and sandstones overlying the basal pale grey mudstone exhibit a coarsening upward trend in grain size, indicating a continuous deposition during the transition from the Youganwo Fm to the Huangniuling Fm. 4), the characteristic sedimentary rhythms of the investigated section may also be used as an additional constraint. In fact, the occurrence of sedimentary rhythms is not unique at the studied section. A marine succession of similar age in Massignano, Italy also displays striking limestone/marl cycles (Jovane et al., 2006). Cyclic lithologic patterns are also seen in the middle Eocene oil shale-bearing lacustrine succession in the Mudurnu-Göynük Basin, Turkey (Ocakoğlu et al., 2012), the Eocene oil shale-bearing Green River Formation in the United States (Meyers, 2008), and other terrestrial records of similar ages in Asia (e.g., Dupont-Nivet et al., 2007; Xiao et al., 2010). All these lithologic cycles are attributed to orbital forcing and represent orbital cycles (Jovane et al., 2006; Dupont-Nivet et al., 2007; Meyers, 2008; Xiao et al., 2010; Ocakoğlu et al., 2012). The strong lithologic expression of orbital variations in both marine and terrestrial records, particularly those containing oil shales, from widespread regions at similar ages leads us to believe that the sedimentary cycles of the studied section likely represent orbital cycles as well. In particular, spectral analysis of magnetic susceptibility depth series of the Youganwo Fm reveals dominant sedimentary cycles with a cycle wavelength ratio of ~4:1, which is in the orbital frequency bands. Therefore, although it is not certain yet as to exactly which orbital cycle(s) (i.e., eccentricity, obliquity, or precession) these sedimentary rhythms may represent, the frequency of these lithologic cycles should be within the orbital frequency bands, which can be used as an additional, first-order constraint when establishing a time scale for the studied section. Based on the definition of the magnetozones (Fig. 8), there are ~3.5 sedimentary cycles in N1. Because a sedimentary cycle in the Huangniuling Fm is represented by a sequence of red layer, massive sandstone, and a thin mudstone, one red layer marker at 40 m might be unidentified, where the accompanied thin mudstone bed did occur (Fig. 8). Therefore, there are probably 4 sedimentary cycles in N1 zone. Similarly, there are ~ 3 sedimentary cycles in R2 zone and ~8.5 sedimentary cycles in N2 zone, respectively (Fig. 8).

5.3 Construction of a geomagnetic polarity timescale (GPTS)

With the aforementioned 4 constraints, correlations between the four polarity zones (Fig. 8e) and the magnetochrons C18r to C13r (Fig. 8f) can be examined and unrealistic correlations can be rejected. Because polarity zones N1 and R2 are better defined than other two polarity zones, correlation is thus constructed mainly between the N1 and R2 pair and the consecutive normal and reversed magnetochrons of the GPTS. To facilitate the analyses, the N2 zone is also used, but as a secondary constraint, in establishing the correlations.

The results of correlations are summarized in Table 1. With the first-order constraint that the Youganwo oil shales were formed in the late Eocene, i.e., from C18 to C13, six ensembles of correlations are possible (Table 1). Ensemble 1 correlates N1 and R2 zones with C18n and C18r, respectively. Ensemble 2 correlates N1 and R2 zones with C17n and C17r, respectively. Ensemble 3 relates N1 to C16n.2n and R2 to C16r. Ensemble 4 links N1 to C16n.1n, R2 to C16n.1r, and N2 to C16n.2n. In Ensemble 5, N1 and R2 zones are correlated to C15n and C15r, respectively. And Ensemble 6 correlates N1 to C13n and R2 to C13r. The quality of each correlation is assessed by examining whether and to what extent the above four constraints are met. The one that satisfies most or all of the constraints is preferred and is used to establish the magnetic polarity timescale for the investigated section. For instance, Ensemble 1 is rejected because this correlation would force the majority of the Youganwo oil shale section (N2-N3), where funa fossils of late Eocene age were discovered, to the middle Eocene (Fig. 8e,f). Ensembles 2 and 3 are rejected on the grounds that the sedimentation rate for N1 in the coarse sandstones is slower than or similar to that of R2 in the oil shale, which violates constraint 2). Ensemble 4 is also rejected because the sedimentation rate for the upper part of the Youganwo Fm (R2) is almost two times that of the lower part of the Youganwo oil shale, which is incompatible with the subtle compositional change within the studied Youganwo Fm.

For Ensemble 5, assuming that C16n.1r was not captured probably due to its relatively short duration, N2 zone would correlate to C16n. Such a correlation yields a sedimentation rate of ~ 6.37 cm/kyr for N1, ~1.75 cm/ky for R2, and ~1.51 cm/kyr for N2 (Table 1). These sedimentation rates comply with the constraints specified in Section 5.2. However, the sedimentation rates of ~1.51 to 1.75 cm/kyr are probably too fast for the investigated oil shale because oil shale in the Youganwo Fm was formed in a semi-deep to deep lake environment (Guo, 1996) and the lithology of the investigated interval of the Youganwo Fm is nearly

monotonic, consisting of only oil shale. A pure shale unit represents a condensed time interval and should be accumulated at very slow rates. Two well-dated organic-rich black shale intervals in the mid-Cretaceous could serve as useful analog to oil shale of the investigated section. The well-dated black shale unit at ~120 Ma is about 5 m thick and represents ~1270 kyr (Li et al., 2008), and thus was accumulated at a rate of ~0.39 cm/kyr. Similarly, the sedimentation rates of the well-dated black shale unit at ~94 Ma (Sageman et al., 2006) are estimated to be ~0.37 to ~0.50 cm/kyr. In addition, Ensemble 5 correlation would result in a duration of 295 kyr (C15n) for N1 zone and 411 kyr for R2 zone. Because there are ~4 and ~3 sedimentary cycles in N1 zone and R2 zone, respectively, the sedimentary cycle in N1 zone and R2 zone would represent a ~74 kyr and ~137 kyr cycle, respectively. The ~137 kyr cycle in R2 zone could be a result of modulation by short eccentricity of orbital variations. But the ~70 kyr cycle in N1 zone is not in the frequency band of orbital variations and its origin is thus difficult to interpret. Therefore, Ensemble 5 is rejected as well.

Ensemble 6 satisfies the constraints on sedimentation rates for the Huangniuling Fm and the Youganwo Fm. Also, the sedimentation rates of 0.42 to 0.56 cm/kyr for the Youganwo Fm (Table 1) are compatible with those of the well-dated, organic-rich black shales in the mid-Cretaceous. Furthermore, this correlation would result in durations of N1, R2, and N2 zones that are largely comparable to those estimated from sedimentary cycles. With ensemble 6 correlation, N1, R2, and N2 zone would represent ~548 kyr, ~1294 kyr, and ~3334 kyr, respectively. Since N1 zone contains ~ 4 sedimentary cycles (Fig. 8a, b), each cycle would represent a ~137 kyr cycle, which is similar to the short eccentricity cycle E2 (95 to 125 kyr). Similarly, since there are ~3 sedimentary cycles in R2 zone (Fig. 8a, b), each sedimentary cycle would represent a ~431 kyr cycle, which is similar to the long eccentricity cycle E1 (405 to 413 kyr). As an additional check, the duration of the sedimentary cycles within N2 zone is calculated. There are ~8.5 sedimentary cycles in N2 zone representing ~3334 kyr and thus each sedimentary cycle has a duration of 392 kyr, which is similar to the periodicity of long eccentricity cycle E1. Therefore, the sedimentary cycles in the Youganwo Fm are consistently shown as representing the long eccentricity cycles. It is reasonable that the sedimentary cycles in N1, i.e., Huangniuling Fm, represent short eccentricity E2 and sedimentary cycles in R2represent long eccentricity E1 because the sedimentation rates of the Huangniuling Fm is much faster than that of the Youganwo Fm and orbital cycles with shorter durations can be recorded in the Huangniuling Fm. Indeed, among these six ensembles, only Ensemble 6 can yield periodicities of all the sedimentary cycles, which are from

different parts of the section, in the orbital frequency band within uncertainties (Table 1). Thus, taking together, Ensemble 6 can satisfy different aspects of major constraints within uncertainties and thus is acceptable.

Analyses of the six possible correlations lead to a conclusion that only Ensemble 6 correlation offers the most realistic scenario. Therefore, the Ensemble 6 correlation is employed to establish a chronologic framework for the studied section (Fig. 8e, f). With this chronologic framework, the transition from the Youganwo Fm to the Huangniuling Fm took place within magnetochron C13r (Fig. 8). Because the transition is represented by a ~ 50 cm thick, mudstone-dominated interval and the C13n/C13r boundary (33.705 Ma) occurs at ~70 cm above the top of the transitional interval, the age of the onset of the transition can be determined by estimating the duration of the ~ 1.2 m thick interval. There are two ways to estimate the duration of the 1.2 m thick interval. One is to extrapolate the sedimentation rate of ~0.56 cm/kyr for the uppermost part of the Youganwo Fm, i.e., R2 zone. This would lead to an estimate of ~210 kyr and the onset of the transition is then estimated to be at ~33.915 Ma. The second approach is to treat the 1.2 m thick interval as the upper part of the long eccentricity cycle at the uppermost of the Youganwo Fm (Fig. 8a, b). This results in an estimate of ~ 140 kyr for the 1.2 m thick interval and an onset age of ~ 33.845 Ma. Taking the average of the above two estimates, we obtain a mean age of 33.88 Ma for the onset of the transition. In summary, the constructed timescale represents a significantly refined chronology for the Paleogene strata in Maoming Basin, and provides the tightest possible constraints on the timing of the onset of the transition from a lacustrine environment to a deltaic environment in the Maoming Basin.

5.4 Paleoclimatic implications

The rapid transition from a lacustrine environment to a deltaic environment could be related to global climate change. In the late Paleogene, the Earth's climate underwent a major transition from greenhouse to icehouse that was climaxed at the Eocene–Oligocene boundary (Zachos et al., 2001). This climatic transition was accompanied by rapid ice sheet growth on the Antarctic (e.g., DeConto and Pollard, 2003; Coxall et al., 2005; Goldner et al., 2014) and was characterized by pronounced global cooling (e.g., Zanazzi et al., 2007; Liu et al., 2009; Bohaty et al., 2012; Hren et al., 2013). The Eocene–Oligocene transition (EOT) was dated at 33.714 Ma (Jovane et al., 2006) or 33.9 ±0.05 Ma (Brown et al., 2009) from the marine succession in Massignano, Italy, which is the Global Stratotype Section and Point (GSSP) for

the Eocene–Oligocene boundary. Studies of the equatorial Pacific records constrain the EOT at ~33.79 Ma (Pälike et al., 2006) or 33.89 Ma (Westerhold et al., 2014). The rapid transition from a lacustrine environment to a deltaic environment in Maoming Basin is dated at 33.88 Ma, which coincides well with the timing of the EOT determined from marine records. The close timing suggests strong linkage between the drastic environmental transition in Maoming Basin and the EOT (Fig. 8f). The dramatic shift from a lacustrine to a deltaic environment at the Maoming Basin suggests that low-latitude Asia likely underwent a transition in regional hydrological cycle from humid to dry conditions in response to global cooling at the EOT. As dry conditions become prevailed, lake level likely dropped and lake area became shrunk. The prevailing drying conditions together with global cooling during EOT probably promoted erosions in upland and supplied abundant sediments to the shrinking lake, leading to the rapid increase in sediment accumulation rates after the dramatic environmental change. The dry conditions perhaps persisted in low-latitude Asia after the dramatic environmental change as the global climate continued to deteriorate following the rapid, severe, and widespread climatic transition at the Eocene–Oligocene boundary (Fig. 7f). This persisted dry condition is indicated by the accumulation of the sandstone-dominated Huangniuling Fm in the Maoming Basin at relatively increased sedimentation rates. Indeed, similar depositional environmental change and increase in sedimentation rates between 34.5 Ma and 31 Ma are also observed in Xining Basin and the E/O climatic transition is considered as a possible cause (Dai et al., 2006).

The new, significantly refined chronology also indicates that the striking sedimentary cycles in both the Youganwo Fm and the Huangniuling Fm likely represent eccentricity cycles. The recognition of eccentricity signal suggests that sedimentation in the Maoming Basin during this time interval may have been modulated by orbital variations, probably via lake level fluctuations at orbital frequency. The occurrence of eccentricity signals in the records is consistent with the fact the Maoming Basin is situated in the low-latitude areas that are sensitive to orbital variations at eccentricity frequency bands. Indeed, modulation of orbital variations on sedimentation appeared to be widespread during this time interval. The long and short eccentricity signals are also detected from the Eocene/Oligocene Massignano section in Italy (Jovane et al., 2006). The eccentricity signals are also found in other marine successions (e.g., Westerhold et al., 2014) and lacustrine deposits (e.g., Meyers, 2008; Okacoğlu et al., 2012) at the similar ages. Therefore, the drastic environmental change in the Maoming Basin during EOT represents the terrestrial responses in low-latitude Asia to the EOT that may be

superimposed on the long-term variations at orbital frequency. The investigated section in the Maoming Basin thus likely faithfully recorded the impacts of the EOT on low-latitude Asia. With the significantly refined chronology, future studies using various proxies shall shed new lights into understanding these regional processes.

6 Conclusions

We have carried out a detailed stratigraphic and paleomagnetic investigation of the upper Paleogene succession in the Maoming Basin, southern China. The investigated succession comprises oil shale dominated Youganwo Fm and the overlying sandstone dominated Huangniuling Fm. Both the Youganwo Fm and the overlying Huangniuling Fm exhibit striking sedimentary rhythms. The sedimentary rhythms of the Youganwo Fm are well expressed the high-resolution magnetic susceptibility (MS) data and spectral analysis of the MS depth series reveals that the dominant meter-scale sedimentary cycles are in orbital frequency bands. The sedimentary rhythms in the Huangniuling Fm are characterized by the repeated occurrence of a parasequence containing red sandstone layer, massive coarse sandstones, and a relatively thin mudstone. New paleomagnetic results, together with the lithologic and fossil age data, allow us to establish a magnetostratigraphy for the studied section that constrains the striking sedimentary rhythms of the Youganwo Fm and Huangniuling Fm to long and short eccentricity cycles, respectively. Taken together, a significantly refined chronologic framework is established for the investigated succession.

The contact between the Youganwo Fm and the Huangniuling Fm is represented by a 50 cm interval that shows a gradual change from dark grey mudstone at the uppermost of the Youganwo Fm to the grey mudstone and siltstones with a coarsening upward trend in grain size at the base of the Huangniuling Fm. This interval represents a major environment change from a lacustrine to a deltaic environment in the Maoming Basin and its onset is dated at ~33.88 Ma. The timing of the onset of the dramatic environmental change is in remarkable similarity with that of the Eocene–Oligocene transition (EOT) that is dated at 33.7 to 33.9 Ma from various marine records. The synchroniety suggests strong linkage between these two events and implies that the rapid environmental change in the Maoming Basin most likely represents terrestrial responses to the global cooling associated with the EOT. This notion is strengthened by the subsequent occurrence of the persistently prolonged dry conditions, as represented by the sandstone-dominated Huangniuling Fm, following the rapid environment

change coincident with the EOT. These features are highly compatible with the continued deteriorating conditions after the EOT.

Acknowledgements

This study was supported by National Natural Science Foundation of China (Nos. 41210001, 41372002, 41274071, 41230208, 41321062, 41528201), the National Basic Research Program of China (No. 2012CB822000), and the Fundamental Research Funds for the Central Universities (20620140389). We thank Shipeng Wang for field assistance, Mike Jackson and Qingsong Liu for helpful discussions about the rock magnetic data. We are grateful to reviewers Alexis Licht, Christian Rolf, and Luigi Jovane whose comments were helpful in improving the manuscript.

References

Aleksandrova, G. N., Kodrul, T. M., Liu, X. Y., Song, Y. S., and Jin. J. H.: Palynological characteristics of the upper part of the Youganwo Formation and lower part of the Huangniuling Formation, Maoming Basin, South China. In Proceedings of the 2nd Sino-Russian Seminar on Evolution and Development of Eastern Asia Flora based on Palaeobotanical Data, 3–15, Guangzhou, China. School of Life Sciences, Sun Yat-sen University, Guangzhou, China, 2012.

Bohaty, S. M., Zachos, J. C. and Delaney, L. M.: Foraminiferal Mg/Ca evidence for Southern Ocean cooling across the Eocene–Oligocene transition. Earth Planet. Sci. Lett. 317–318, 251–261, 2012.

Bureau of Geology and Mineral Resources of Guangdong Province: Regional Geology of Guangdong Province. Geological Publishing House, Beijing. (In Chinese with English abstract), 1988.

Bureau of Geology and Mineral Resources of Guangdong Province: Stratigraphy (Lithostratic) of Guangdong Province. China University of Geosciences Press, Wuhan. (In Chinese), 1996.

Brown, R. E., Koeberl, C., Montanari, A., and Bice, D. M.: Evidence for a change in Milankovitch forcing caused by extraterrestrial events at Massignano, Italy, Eocene-Oligocene boundary GSSP, in: The Late Eocene Earth – Hothouse, Icehouse and Impacts, edited by: Koeberl, C., and Montanari, A., Geol. S. Am. S., 452, 119–137, doi:10.1130/2009.2452(08), 2009.

Chang, L., Robert, A.P., Rowan, C.J., Tang, Y., Pruner, P., Chen, Q., and Horng, C.S., Low-temperature magnetic properties of greigite (Fe_3S_4). Geochem. Geophys. Geosyst., 10, Q01Y04, doi:10.1029/2008GC002276, 2007.

Chow M.C., On some Eocene and Oligocene mammals from Kwangsi and Yunnan. Verterbrata PalAsiatica, 1(3): 201-214, 1957 (in Chinese with English abstract).

Chow, M.C., Liu, C.L.: A new anosterine turtle from Maoming, Kwangtung. Acta Palaeontologica Sinica 3 (4), 275–282, 1955 (In Chinese with English abstract).

Chow, M.C., Yeh, H.K., A new emydid from the Eocene of Maoming, Kwangtung. Vertebrata Palasiatica 6 (3), 225–229, 1962 (In Chinese with English abstract).

Claude, J., Zhang, J.Y., Li, J.J., Mo, J.Y., Kuang, X.W., and Tong, H.Y.: Geoemydid turtles from the Late Eocene Maoming basin, southern China. Bull. Soc. géol. France 183 (6), 641-651, 2012.

Coxall, H. K., Wilson, P. A., Pa¨like, H., Lear, C. H. and Backman, J.: Rapid stepwise onset of Antarctic glaciation and deeper calcite compensation in the Pacific Ocean. Nature 433, 53–57, 2005.

Cotton, L.J., and Pearson, P.N.: Extinction of larger benthic foraminifera at the Eocene/Oligocene boundary. Palaeogeography, Palaeoclimatology, Palaeoecology 311, 281–296, 2011.

Dai, S., X. Fang, G. Dupont-Nivet, C. Song, J. Gao, W. Krijgsman, C. Langereis, and W. Zhang (2006), Magnetostratigraphy of Cenozoic sediments from the Xining Basin: Tectonic implications for the northeastern Tibetan Plateau, J. Geophys. Res., 111, B11102, doi:10.1029/2005JB004187.

Danilov I. G., Syromyatnikova E. V., Skutschas P. P., Kodrul T. M. and Jin J. H.: The first 'True' Adocus (Testudines, Adocidae) from the Paleogene of Asia, Journal of Vertebrate Paleontology 33(5), 1071–1080, 2013.

DeConto, R. M. and Pollard, D.: Rapid Cenozoic glaciation of Antarctica induced by declining atmospheric CO2. Nature 421, 245–249, 2003.

Dunlop, D. J., and Ö. Özdemir: Rock Magnetism: Fundamentals and Frontiers, 573 pp., Cambridge Univ. Press, Cambridge, U. K., 1997.

Dupont-Nivet, G., Krijgsman, W., Langereis, C. G., Abels, H. A., Dai, S., and Fang, X. M.: Tibetan plateau aridification linked to global cooling at the Eocene – Oligocene transition, Nature 445, 635–638, 2007.

Feng, X. X., Oskolski, A., and Jin, J.H.: Eocene dicotyledonous wood, Bischofia maomingensis sp. nov. from Maoming Basin, South China. Review of Palaeobotany and Palynology 174, 101–105, 2012.

Feng, X. X., Tang, B., Kodrul, T. M., and Jin, J.H.: Winged fruits and associated leaves of Shorea (Dipterocarpacesa) from the late Eocence of South China and their phytogeogrpahic and paleoclimatic implications. American Journal of Botany 100(3), 574 – 581, 2013.

Goldner, A., Herold, N. and Huber, M.: Antarctic glaciation caused ocean circulation changes at the Eocene–Oligocene transition. Nature 511, 574-577, doi:10.1038/nature13597, 2014.

Guo, M.: Characteristics and mineralization controlling factors of oil shale in Maoming Basin. M.sc. Thesis, Jilin University, p 86. 2006.

Hren, M. T., Sheldonc, N.D., Grimesd, S.T., Collinsone, M. E., Hookerf, J.J., Buglerd, M., and Lohmannc, K. C.: Terrestrial cooling in Northern Europe during the Eocene–Oligocene transition. Proc. Natl Acad. Sci. 110, 7562–7567, 2013.

Huang X.S., New emoropid (Mammalia, Perissodactyla) remains from the middle Eocene of Yuanqu Basin. Verterbrata PalAsiatica, 40(4): 286-290, 2002 (in Chinese with English abstract).

Huang X., Qi T., Notes on Late Eocene Tapiroids from the Lunan Basin, eastern Yunnan. Verterbrata PalAsiatica, 20(4): 315-326, 1982 (in Chinese with English abstract)

Jelinek, V.: Characterization of the magnetic fabrics of rocks, Tectonophysics 79, 63– 67, 1981.

Jin, J.H.: On the age of the Youganwo Formation in the Maoming Basin, Guangdong Province. Journal of Stratigraphy 32 (1), 47–50 (In Chinese with English abstract), 2008.

Jovane, L., F. Florindo, M. Sprovieri, and H. Pälike: Astronomic calibration of the late Eocene/early Oligocene Massignano section (central Italy), Geochem. Geophys. Geosyst. 7, Q07012, doi:10.1029/2005GC001195, 2006.

Kirschvink, J. L.: The least-squares line and plane and the analysis of paleomagnetic data, Geophys. J. Int. 62, 699–718, doi: 10.1111/j.1365-246X.1980.tb02601.x., 1980.

Li C., Ting S., The Paleogene mammals of China. Bull. Bulletin of Carnegie Museum of Natural History, 21: 1-93, 1983 (in Chinese with English abstract).

Li, J.L.: New materials of Tomistoma petrolica Yeh from Maoming, Guangdong. Vertebrata Palasiatica 13 (3), 190–194 (In Chinese), 1975.

Li, Y.X., T.J. Bralower, I.P. Montanez, D.A. Osleger, M.A. Arthur, D.M. Bice, T.D. Herbert, E. Erba, I. Premoli-Silva: Toward an orbital chronology for the early Aptian Oceanic Anoxic Event 1a (OAE1a, ~120 Ma). Earth and Planetary Science Letters 271, 88–100. doi:10.1016/j.epsl.2008.03.055, 2008.

Licht, A. van Cappelle, M., Abels, H. A., Ladant, J.-B., Trabucho-Alexandre, J., France-Lanord, C.: Asian monsoons in a late Eocene greenhouse world. Nature 513, 501-506. doi:10.1038/nature13704, 2014.

Licht, A., Boura, A., De Franceschi, D., Utescher, T., Sein, C., and Jaeger, J.-J.: Late middle Eocene fossil wood of Myanmar: Implications for the landscape and the climate of the Eocene Bengal Bay. Review of Palaeobotany and Palynology 216, 44–54, 2015.

Liu, X.T.: A new fossil cyprinid fish from Maoming, Kwangtung. Vertebrata Palasiatica 1 (2), 151–153 (In Chinese with English abstract), 1957.

Liu, Z.H., Pagani, M., Zinniker, D., DeConto, R., Huber, M., Brinkhuis, H., Shah, S.R., Leckie, R.M. and Pearson, A.: Global cooling during the Eocene–Oligocene climate transition. Science 323, 1187–1190, 2009.

Lowrie, W.: Identification of ferromagnetic minerals in a rock by coercivity and unblocking temperature properties, Geophys. Res. Lett., 17, 159–162, 1990.

Lurcock, P. C., and G. S. Wilson: PuffinPlot: A versatile, user-friendly program for paleomagnetic analysis, Geochem. Geophys. Geosyst. 13, Q06Z45, doi:10.1029/2012GC004098, 2012.

McFadden, P.L., and McElhinny, M.W.: Classification of the reversal test in palaeomagnetism. Geophys. J. Int. 103,725-729, 1990.

Meyers, S.R.: Resolving Milankovitchian controversies: The Triassic Latemar Limestone and the Eocene Green River Formation. Geology 36, 319–322, doi: 10.1130/G24423A.1, 2008.

Muller, R.A. and MacDonald, J.G.: Ice ages and astronomical causes: Data, spectral analysis, and mechanisms. Springer Praxis, Berlin, 2000.

Ocakoğlu, F., Açıkalın, S., Yılmaz, I.Ö., Safak, Ü., and Gökçeoglu, C.: Evidence of orbital forcing in lake-level fluctuations in the Middle Eocene oil shale-bearing lacustrine successions in the Mudurnu-Göynük Basin, NW Anatolia (Turkey). Journal of Asian Earth Sciences 56, 54–71, 2012.

Ogg, J.G., Chapter 5: Geomagnetic Polarity Time Scale: in Gradstein, F.M., Ogg, J.G., Schmitz, M.D., and Ogg, G.M., eds., The Geologic Time Scale 2012, Elsevier, Amsterdam, 85–113, 2012.

Oskolski A. A., Feng X. X., Jin J. H.: Myrtineoxylon gen. nov.: The first fossil wood record of the tribe Myrteae (Myrtaceae) in eastern Asia. Taxon 62 (4), 771–778, 2013.

Özdemir, Ö., Dunlop, D.J., and Moskowitz, B.M. The effect of oxidation on the Verwey transition in magnetite. Geophysical Research Letters, 20, 1671-1674, doi:10.1029/93/GL01483, 1993.

Pälike, H., Norris, R. D., Herrle, J. O., Wilson, P. A., Coxall, H. K., Lear, C. H., Shackleton, N. J., Tripati, A. K., and Wade, B. S.: The Heartbeat of the Oligocene Climate System, Science 314, 1894–1898, doi:10.1126/science.1133822, 2006.

Pälike, H., Lyle, M. W., Nishi, H., Raffi, I., Ridgwell, A., and Gamage, K., et al.: A Cenozoic record of the equatorial Pacific carbonate compensation depth, Nature 488, 609–614, doi:10.1038/nature11360, 2012.

Pearson, P.N., McMillan, I.K., Wade, B.S., Dunkley Jones, T., Coxall, H.K., Bown, P.R., Lear, C.H.: Extinction and environmental change across the Eocene–Oligocene boundary in Tanzania. Geology 36, 179–182, 2008.

Prothero, D.R.: The late Eocene-Oligocene extinctions. Annu. Rev. Earth Planet. Sci. 22, 145-165, 1994.

Qiu Z.X., Wang B., Paracerathere fossils of China. Palaeontoligca Sinica, New Ser. C, 29: 1-188, 2007 (in Chinese with English abstract).

Quan, C., Liu, Z.H., Utescher, T., Jin, J.H., Shu, J.W., Li, Y.X., Liu, Y.-S. C: Revisiting the Paleogene climate pattern of East Asia: A synthetic review. Earth-Science Reviews 139, 213–230, 2014.

Quan, C., Liu, Y.-S.C. and Utescher, T.: Eocene monsoon prevalence over China: a paleobotanical perspective. Palaeogeogr. Palaeoclimatol. Palaeoecol. 365–366, 302–311, 2012.

Roberts, A. P., L. Chang, C. J. Rowan, C. - S. Horng, and F. Florindo: Magnetic properties of sedimentary greigite (Fe3S4): An update. Rev. Geophys. 49, RG1002, doi:10.1029/2010RG000336, 2011.

Russell D.E., Zhai R.J., The Paleogene of Asia: mammals and stratigraphy. Memoires du Museum National d'Histoire Naturelle, 52: 1-490, 1987.

Sageman, B.B., Meyers, S.R., and Arthur, M.A.: Orbital time scale and new C-isotope record for Cenomanian-Turonian boundary stratotype. Geology 34, 125–128, doi:10.1130/G22074.1, 2006.

Shukla, A, Mehrotra, R.C., Spicer, R.A, Spicer, T.E.V., and Kumara, M.: Cool equatorial terrestrial temperatures and the South Asian monsoon in the Early Eocene: Evidence from the Gurha Mine, Rajasthan, India. Palaeogeogr. Palaeoclimatol. Palaeoecol. 412, 187–198, 2014.

Skutschas P. P., Danilov I. G., Kodrul T. M. and Jin J. H.: The First Discovery of an Alligatorid (Crocodylia, Alligatoroidea, Alligatoridae) in the Eocene of China. Journal of Vertebrate Paleontology 34(2), 471–476, 2014.

Snowball I. F. and Torii, M., Incidence and significance of magnetic iron sulphides in Quaternary sediments and soils, in Quaternary Climates, Environments and Magnetism, edited by B.A. Maher and R. Thompson, pp. 199-230. Cambridge Univ. Press, Cambridge, U.K., doi:10.1017/CBO9780511535635.009, 1999

Tauxe, L.: Paleomagnetic principles and practice, 301 pp., Kluwer Academic Publisher, 1998.

Tong Y., Zheng S., Qiu Z., Cenozoic mammal ages of China. Verterbrata PalAsiatica, 33(4): 290-314, 1995 (in Chinese with English abstract).

Tong, Y.S., Li, Q., and Wang, Y. Q.: A brief introduction to recent advance in the Paleogene studies. Journal of Stratigraphy 29 (2), 109-133 (In Chinese with English abstract), 2005.

Tong, Y.S., Li, Q., and Wang, Y. Q.: An introduction to recent advance in the study of the continental Early Paleogene stages in China. Journal of Stratigraphy 37 (4), 428-440 (In Chinese with English abstract), 2013.

Verwey, E. J. W. Electronic conduction of magnetite (Fe_3O_4) and its transition point at low temperatures, Nature, 144, 327-328, doi:10.1038/144327b0. 1939

Wang B., The Chinese Oligocene: A preliminary review of mammalian localities and local faunas. In: Prothero D.R., Berggren W.A., eds. Eocene-Oligocene Climatic and Biotic Evolution. Princeton: Princeton University Press, 529-547, 1992 (in Chinese with English abstract).

Wang B., Problems and recent advances in the division of the continental Oligocene. Verterbrata PalAsiatica, 21(2): 81-90, 1997 (in Chinese with English summary).

Wang, D., Lu, S., Han, S., Sun, X. and Quan, C.: Eocene prevalence of monsoon-like climate over eastern China reflected by hydrological dynamics. J. Asian Earth Sci. 62, 776–787, 2013.

Wang, J.D., Li, H. M., Zhu, Z. Y., Seguin, M. K., Yang, J. F., and Zhang, G. M.: Magnetostratigraphy of Tertiary rocks from Maoming Basin, Guangdong Province, China. Chinese Journal of Geochemistry 13, 165-175, 1994.

Wang, Y.Y., Zhang, Z.H., and Jin, J.H.: Discovery of Eocene fossil mammal from Maoming Basin, Guangdong. Acta Scientiarum Naturalium Universitatis Sunyatseni 46 (3), 131-133 (In Chinese with English abstract), 2007.

Westerhold, T, U. Röhl, H. Pälike, R. Wilkens, P. A. Wilson, and G. Acton: Orbitally tuned timescale and astronomical forcing in the middle Eocene to early Oligocene. Clim. Past, 10, 955–973, doi:10.5194/cp-10-955-2014, 2014.

Xiao, G. Q., Abels, H. A., Yao, Z. Q., Dupont-Nivet, G., and Hilgen, F. J.: Asian aridification linked to the first step of the Eocene-Oligocene climate Transition (EOT) in obliquity-dominated terrestrial records (Xining Basin, China). Clim. Past, 6, 501–513, doi:10.5194/cp-6-501-2010, 2010.

Yeh, H.K.: A new crocodile from Maoming, Kwangtung. Vertebrata Palasiatica 2 (4), 237–242 (In Chinese with English abstract), 1958.

Yu, J.F. and Wu, Z.J.: Spore-pollen assemblage of Mao 5 well of Maoming Basin, Guangdong and its geological age. Journal of Stratigraphy 7 (2), 112-118 (In Chinese), 1983.

Zachos, J.C., Pagani, M., Sloan, L., Thomas, E., and Billups, K.: Trends, rhythms, and aberrations in global climate 65 Ma to present. Science 292, 686–693, 2001.

Zanazzi, A., Kohn, M.J., MacFadden, B.J., and Terry, D.O. Jr.: Large temperature drop across the Eocene–Oligocene transition in central North America. Nature 445, 639–642, 2007.

Zijderveld, J.D.A.: A. C. demagnetization of rocks: analysis of results, in Methods in Palaeomagnetism, pp. 254–286, edited by D.W. Collinson, K.M. Creer and S.K. Runcorn, Elsevier, Amsterdam, 1967.

Zong G., Cenozoic Mammals and Environment of Hengduan Mountains Region. China Ocean Press, Beijing, 279, 1996 (in Chinese with English abstract).

Table 1 Correlations of magnetozones with Chrons C18 to C13 of the geomagnetic polarity time scale (GPTS).

Note:

*, N1 is defined from 32.2 to 51.0 m and contains ~ 4 sedimentary cycles; R2 is defined from 25.0 to 32.2 m and contains ~3 sedimentary cycles; N2 is defined from 11.0 to 25.0 m and contains ~8.5 sedimentary cycles. Bold (regular) fonts indicate normal (reversed) polarity zones/chrons; The two numbers in each cell are sedimentation rate in cm/kyr and the perodicity of the sedimentary cycle (in kyr) calculated based on the correlation. For example, 1.23, 382 in the very first cell indicate that the sedimentation rate is 1.23 cm/kyr and the sedimentary cycle represents 382 kyr based on Correlation 1. "-" denotes "not applicable"; "x" indicates that the correlation is unrealistic and is rejected. " √ " indicates acceptable correlations; a-e provides brief comments on why the correlation is rejected or accepted. a, the correlation would place the majority of the Youganwo Fm, i.e., N2-N3, to the middle Eocene; b, the correlation would result in sedimentation rates in R2, i.e., the Youganwof Fm, faster than or similar to those in N1, i.e., the Huangniuling Fm; c, the correlation leads to the drastic difference in sedimentation rates between the upper (R2) and lower (N2) part of the studied Youganwo Fm; d, the sedimentation rates for the Youganwo oil shale are too fast in comparison to those of well-dated organic-rich shales in deep-time; e, the sedimentation rates of the Youganwo oil shale are compatible with those of well-dated organic-rich shales in deep-time and the sedimentary cycles in both Huangniuling Fm (N1) and the Youganwo Fm (R2 and N2) are in the orbital frequency bands and likely represent eccentricity cycles.

Figure captions

Figure 1 Location and regional geology of the study area. (a) Map showing the location of the Maoming Basin, Guangdong Province, southern China. (b) Simplified geological map of the Maoming Basin. 1. Precambrian; 2. Upper Cretaceous; 3. Youganwo Fm.; 4. Huangniuling Fm.; 5. Shangcun Fm.; 6. Laohuling Fm.; 7. Gaopengling Fm.; 8. Quaternary; 9. Fault; 10. Investigated Jintang section. MR, MB, and MS mark the sites where samples were collected for a magnetostratigraphic study by Wang et al. (1994). See text for details.

Figure 2 Stratigraphy of the investigated section exposed in the now-abandoned open mine pit in Maoming Basin. Lithostratigraphic column (a) shows that the investigated section contains the Youganwo Fm in the lower part and the Huangniuling Fm in the upper part. The Huangniuling Fm part of the stratigraphic column schematically shows the overall rhythmic sedimentary feature that is characterized by the occurrence of a thin bed (shown in short red lines) of red coarse sandstone at the base, followed by massive grey sandstone that is capped by light grey clays.The Youganwo Fm also exhibits sedimentary rhythms that are characterized by repeated occurrence of the beds with distinct reddish color at distance that are indicated by the pinkish lines. Sedimentary cycles (b) are reflected by magnetic susceptibility data. The distinct reddish beds in the Youganwo Fm and the thin red sandstone layers in the Huangniuling Fm generally correspond to the magnetic susceptibility peaks. The distinct thin red sandstone layer in the Huangniuling Fm is numbered and a total of 19 repeated sedimentary packages (cycles) are identified. . Note the different scales of the magnetic susceptibility of the Youganwo Fm (the lower part) and the Huangniuling Fm (the upper part). Field photographs (c-e) show the major sedimentary features of the two formations and the contact between them. In (c), the red arrows indicate the red, thin marker bed of sandstone in the Huangniuling Fm. In (d), the arrow marks the contact between the two formations, displaying a continuous, gradual transition from brown grey mudstones at the uppermost of the Youganwo Fm to pale grey mudstones at the base of the Huangniuling Fm. In (e), the yellow ellipse at the lower-middle part of the picture marks a person (~1.6 m) for scale; red arrows point to several distinctive reddish layers that form the sedimentary rhythms in the Youganwo Fm. br grey = brown grey, lt grey = light grey.

Figure 3 Spectral analysis of the depth series of magnetic susceptibility the Youganwo oil shale. The analysis reveals dominant sedimentary cycles with cycle wavelength ratios similar to periodicity ratios of orbital cycles, suggesting that these sedimentary cycles are orbital frequency bands. The red curve represents the noise level above which the spectral peaks are considered statistically significant. The numbers above the spectral peaks indicate cycle wavelength (in cm) of the sedimentary cycles.

Figure 4 Anisotropy of magnetic susceptibility (AMS) data of the Youganwanwo Fm (a, b) and the Huangniuling Fm (c, d). k1, k2, k3 are the maximum, intermediate, and minimum axis of the anisotropy ellipsoid, respectively. (a, c) are the equal area projection of these

principal axes. No. is the number of specimens. T and Pj in (b, d) are the shape factor and the degree of anisotropy, respectively (Jelinek, 1981).

Figure 5 Rock magnetic data of samples from the Youganwo Fm and Huangniuling Fm. (a) – (e), thermal changes of magnetic susceptibility (MS) of samples from the Huangniuling mudstone (a, b), the uppermost brown grey shale (c) and the oil shale (d, e) of the Youganwo Fm during a heating-cooling cycle between room temperature and 700°C; (f), IRM acquisition and the subsequent demagnetization in a backward DC field; (g-j), Zero-field-cooled (ZFC) and field-cooled (FC) low temperature measurements of the representative samples. The arrow in (g) marks the subdued Verwey transition; (k-o) thermal demagnetization of composite IRM along Z-, Y-, and X-axis at a field of 1.2T, 0.6T, and 0.125T, respectively.

Figure 6 Representative demagnetization data of samples from the studied section. Open/closed squares indicate the vertical/horizontal components.

Figure 7 Characteristic remanent magnetization in stratigraphic coordinates. The solid/open symbols represent the lower/upper hemisphere projection.

Figure 8 Integrated litho-, cyclo-, and magnetostratigraphy of the investigated section, and the correlation with the δ18O and δ13C records from the equatorial Pacific deep-sea sediments (ODP site 1218) (Pälike et al., 2006) that show the Eocene-Oligocene climatic transition (EOT). The legends for lithology and sedimentary cycles are the same as those in Fig. 2. In (c,d), the solid (open) symbols represent “A”(“B”)-quality ChRM data.

Table 1 Correlations of magnetozones with Chrons C18 to C13 of the geomagnetic polarity timescale (GPTS)

		Polarity Chrons/subchrons (duration in myr)														
		C18n	C18r	**C17n**	C17r	**C16n.2n**	C16r	**C16n.1n**	C16n.1r	**C16n.2n**	**C15n**	C15r	**C16n**	**C13n**	C13r	**C15n-C17n**
Correlations	Polarity zone*	**(1.529)**	(1.01)	**(1.363)**	(0.283)	**(0.649)**	(0.269)	**(0.186)**	(0.159)	**(0.649)**	**(0.295)**	(0.411)	**(0.994)**	**(0.548)**	(1.294)	**(3.334)**
1	**N1**	**1.23, 382**	-													
x[a]	R2	-	0.71, 337													
2	**N1**			**1.38, 341**	-											
x[b]	R2			-	2.54, 94											
3	**N1**					**2.90, 162**	-									
x[b]	R2					-	2.68, 90									
	N1							**10.11, 47**	-	-						
4	R2							-	4.53, 53	-						
x[c]	**N2**							-	-	**2.31, 76**						
	N1										**6.37, 74**	-	-			
5	R1										-	1.75, 137	-			
x[d]	**N2**										-	-	**1.51, 117**			
	N1													**3.43, 137**	-	-
6	R1													-	0.56, 431	-
√[e]	**N2**													-	-	**0.42, 392**

Note: *, N1 is defined from 32.2 to 51.0 m and contains ~ 4 sedimentary cycles; R2 is defined from 25.0 to 32.2 m and contains ~3 sedimentary cycles; N2 is defined from 11.0 to 25.0 m and contains ~8.5 sedimentary cycles. Bold (regular) fonts indicate normal (reversed) polarity zones/chrons; The two numbers in each cell are sedimentation rate in cm/kyr and the periodicity of the sedimentary cycle (in kyr) calculated based on the correlation. For example, 1.23, 382 in the very first cell indicate that the sedimentation rate is 1.23 cm/kyr and the sedimentary cycle represents 382 kyr based on Correlation 1. "-" denotes "not applicable"; "x" indicates that the correlation is unrealistic and is rejected. " √ " indicates acceptable correlations; a-e provides brief comments on why the correlation is rejected or accepted. a, the correlation would place the majority of the Youganwo Fm, i.e., N2-N3, to the Middle Eocene; b, the correlation would result in sedimentation rates in R2, i.e., the Youganwof Fm, faster than or similar to those in N1, i.e., the Huangniuling Fm; c, the correlation leads to the drastic difference in sedimentation rates between the upper (R2) and lower (N2) part of the studied Youganwo Fm; d, the sedimentation rates for the Youganwo oil shale are too fast in comparison to those of well-dated organic-rich shales in deep-time; e, the sedimentation rates of the Youganwo oil shale are compatible with those of well-dated organic-rich shales in deep-time and the sedimentary cycles in both Huangniuling Fm (N1) and the Youganwan Fm (R2 and N2) are in the orbital frequency bands and likely represent eccentricity cycles.

Fig. 1

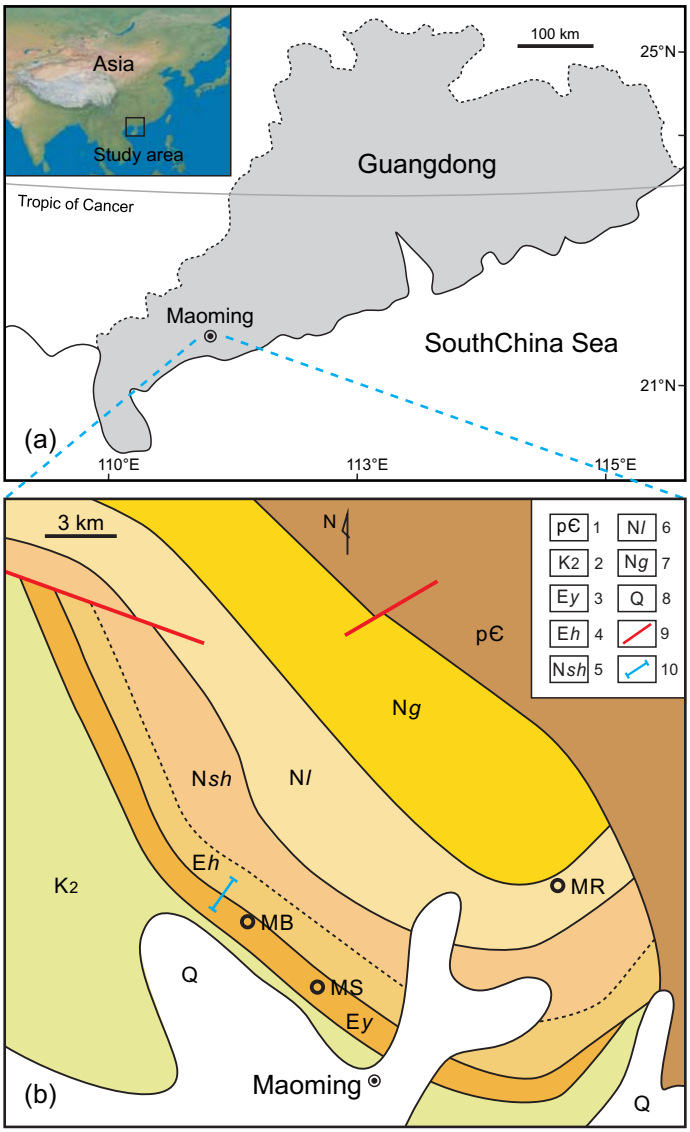
Asia
Study area
100 km
25°N
Guangdong
Tropic of Cancer
Maoming
SouthChina Sea
21°N
(a)
110°E
113°E
115°E
3 km
N
pЄ
Ng
Nsh
N/
Eh
K2
MR
MB
Q
MS
Ey
Maoming
(b)
Q
pЄ 1
K2 2
Ey 3
Eh 4
Nsh 5
N/ 6
Ng 7
Q 8
9
10

Fig. 2

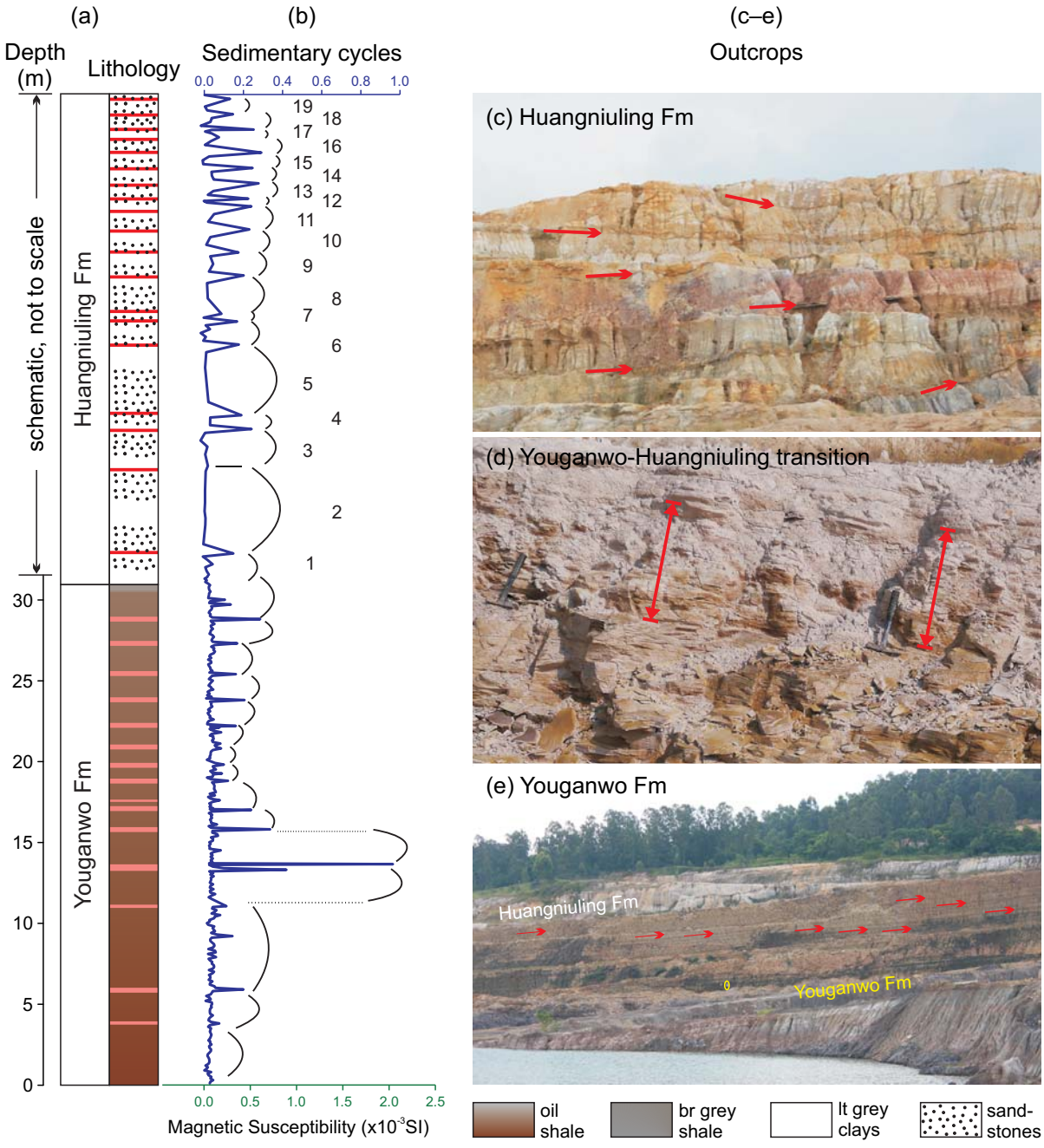
(a)
(b)
(c–e)
Depth (m)
Lithology
Sedimentary cycles
Outcrops
schematic, not to scale
Huangniuling Fm
Youganwo Fm
Magnetic Susceptibility (x10-3SI)
(c) Huangniuling Fm
(d) Youganwo-Huangniuling transition
(e) Youganwo Fm
Huangniuling Fm
Youganwo Fm
oil shale
br grey shale
lt grey clays
sand-stones

Fig. 3

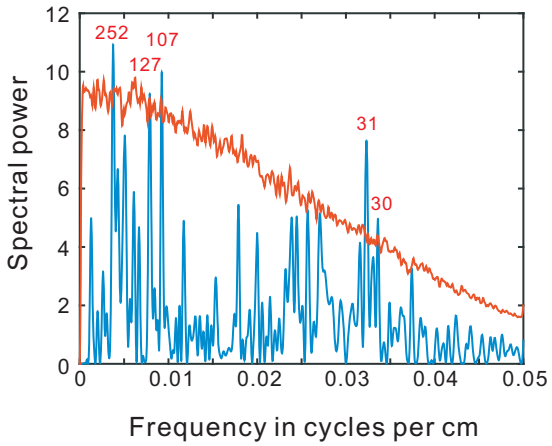
252
107
127
31
30
Spectral power
Frequency in cycles per cm
0
2
4
6
8
10
12
0
0.01
0.02
0.03
0.04
0.05

Fig. 4

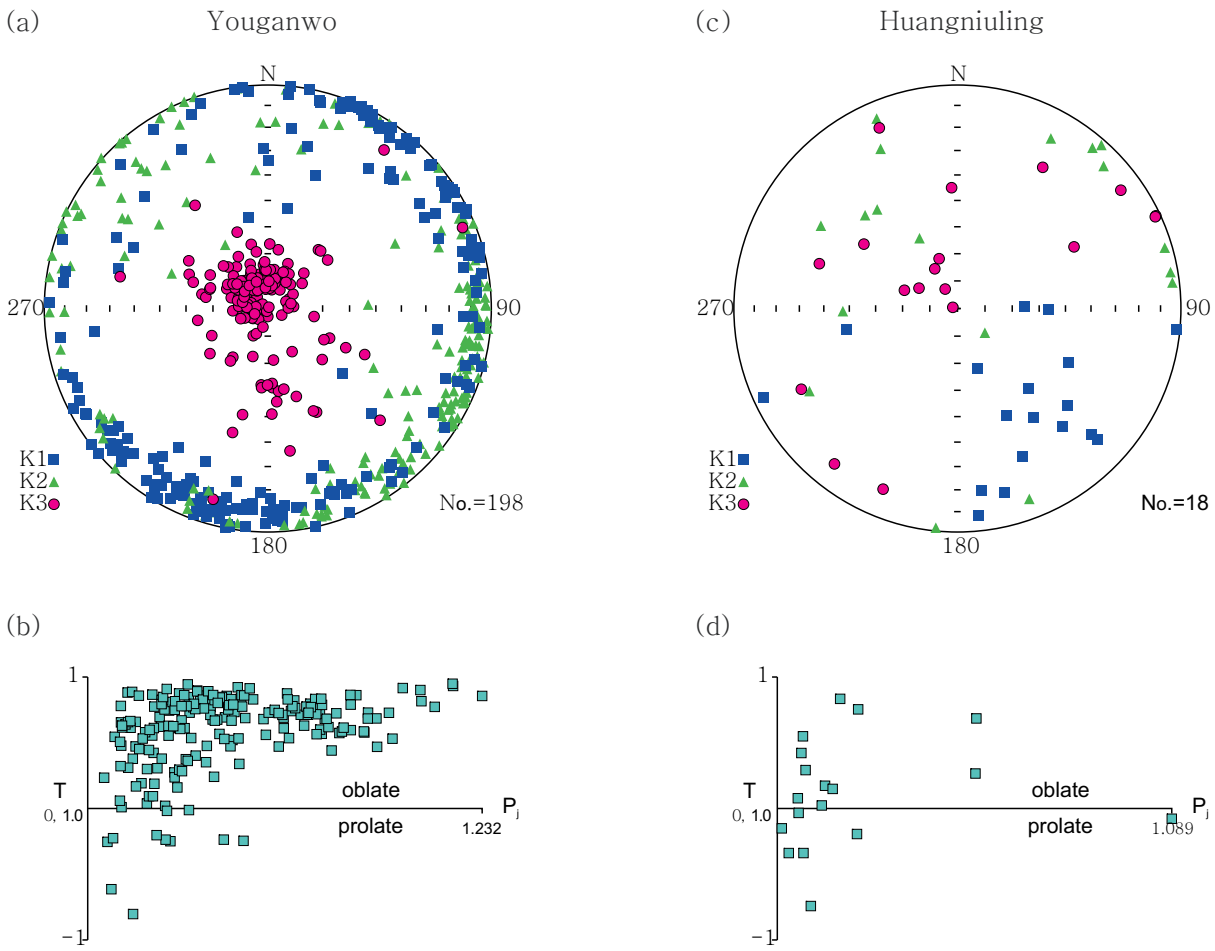
(a)
Youganwo
N
270
90
180
K1
K2
K3
No.=198
(c)
Huangniuling
N
270
90
180
K1
K2
K3
No.=18
(b)
1
T
0, 1.0
oblate
prolate
Pj
1.232
−1
(d)
1
T
0, 1.0
oblate
prolate
Pj
1.089
−1

Fig. 5

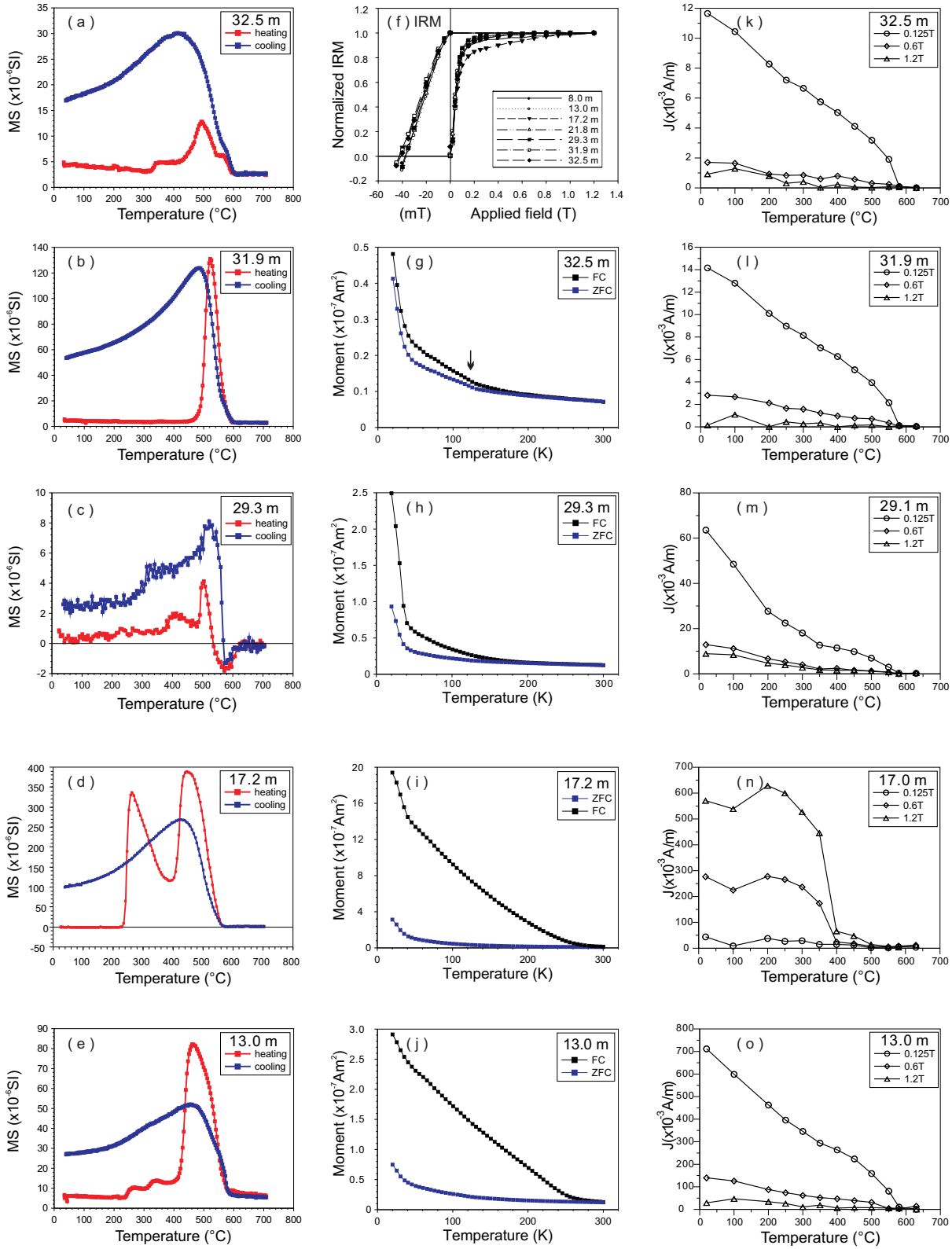
(a)
32.5 m
heating
cooling
MS (x10^{-6}SI)
Temperature (°C)
(b)
31.9 m
heating
cooling
MS (x10^{-6}SI)
Temperature (°C)
(c)
29.3 m
heating
cooling
MS (x10^{-6}SI)
Temperature (°C)
(d)
17.2 m
heating
cooling
MS (x10^{-6}SI)
Temperature (°C)
(e)
13.0 m
heating
cooling
MS (x10^{-6}SI)
Temperature (°C)
(f) IRM
Normalized IRM
8.0 m
13.0 m
17.2 m
21.8 m
29.3 m
31.9 m
32.5 m
(mT)
Applied field (T)
(g)
32.5 m
FC
ZFC
Moment (x10^{-7}Am^2)
Temperature (K)
(h)
29.3 m
FC
ZFC
Moment (x10^{-7}Am^2)
Temperature (K)
(i)
17.2 m
ZFC
FC
Moment (x10^{-7}Am^2)
Temperature (K)
(j)
13.0 m
FC
ZFC
Moment (x10^{-7}Am^2)
Temperature (K)
(k)
32.5 m
0.125T
0.6T
1.2T
J(x10^{-3}A/m)
Temperature (°C)
(l)
31.9 m
0.125T
0.6T
1.2T
J(x10^{-3}A/m)
Temperature (°C)
(m)
29.1 m
0.125T
0.6T
1.2T
J(x10^{-3}A/m)
Temperature (°C)
(n)
17.0 m
0.125T
0.6T
1.2T
J(x10^{-3}A/m)
Temperature (°C)
(o)
13.0 m
0.125T
0.6T
1.2T
J(x10^{-3}A/m)
Temperature (°C)

Fig. 6

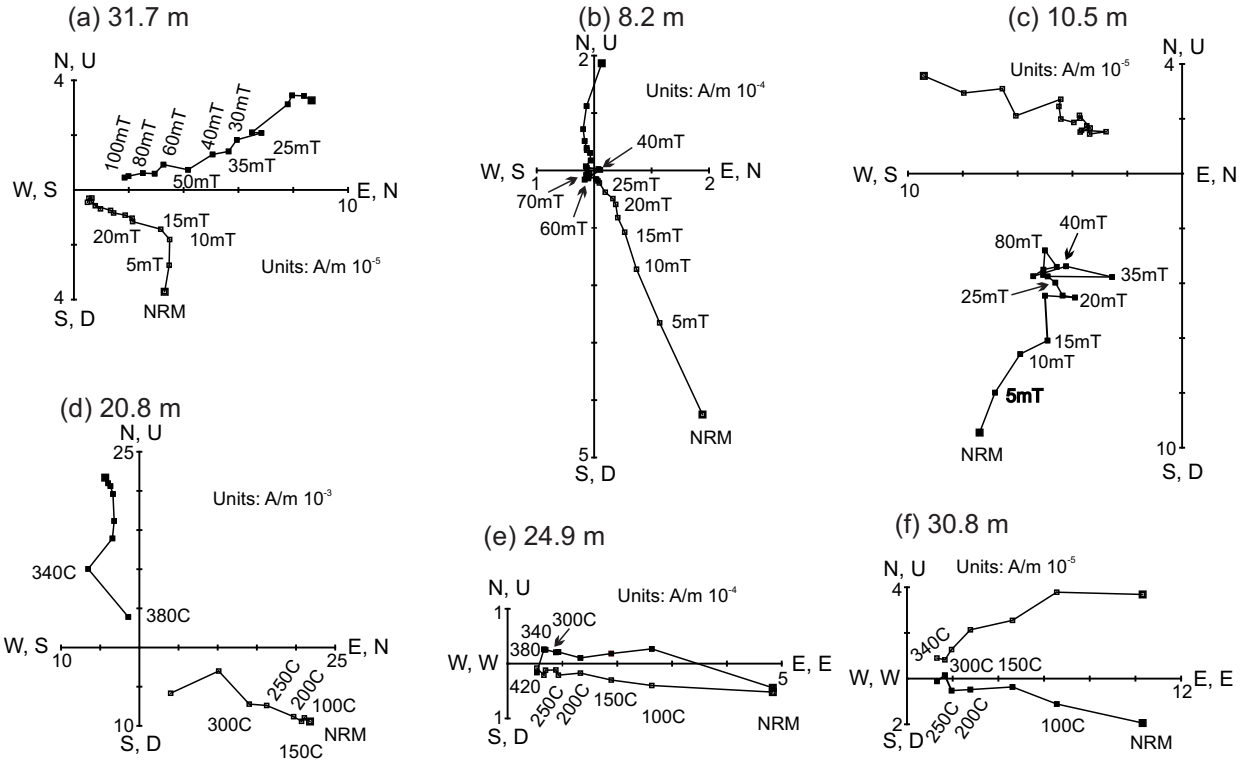
(a) 31.7 m
N, U
4
W, S
E, N
10
S, D
4
100mT
80mT
60mT
40mT
30mT
25mT
35mT
50mT
15mT
20mT
10mT
5mT
NRM
Units: A/m 10-5
(b) 8.2 m
N, U
2
Units: A/m 10-4
W, S
1
2
E, N
40mT
25mT
70mT
20mT
60mT
15mT
10mT
5mT
NRM
5
S, D
(c) 10.5 m
N, U
4
Units: A/m 10-5
W, S
10
E, N
40mT
80mT
35mT
25mT
20mT
15mT
10mT
5mT
NRM
10
S, D
(d) 20.8 m
N, U
25
Units: A/m 10-3
340C
380C
W, S
10
25
E, N
250C
200C
100C
300C
NRM
10
S, D
150C
(e) 24.9 m
N, U
1
Units: A/m 10-4
340
300C
380
W, W
E, E
5
420
250C
200C
150C
100C
NRM
1
S, D
(f) 30.8 m
N, U
Units: A/m 10-5
4
340C
W, W
300C 150C
12
E, E
2
S, D
250C
200C
100C
NRM

Fig. 7

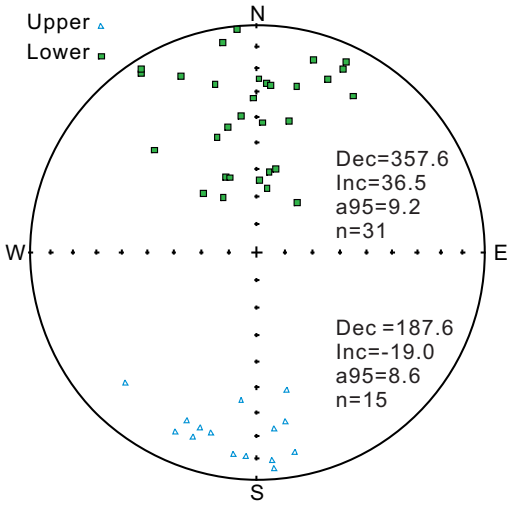
Upper
Lower
N
W
E
S
Dec=357.6
Inc=36.5
a95=9.2
n=31
Dec =187.6
Inc=-19.0
a95=8.6
n=15

Fig. 8

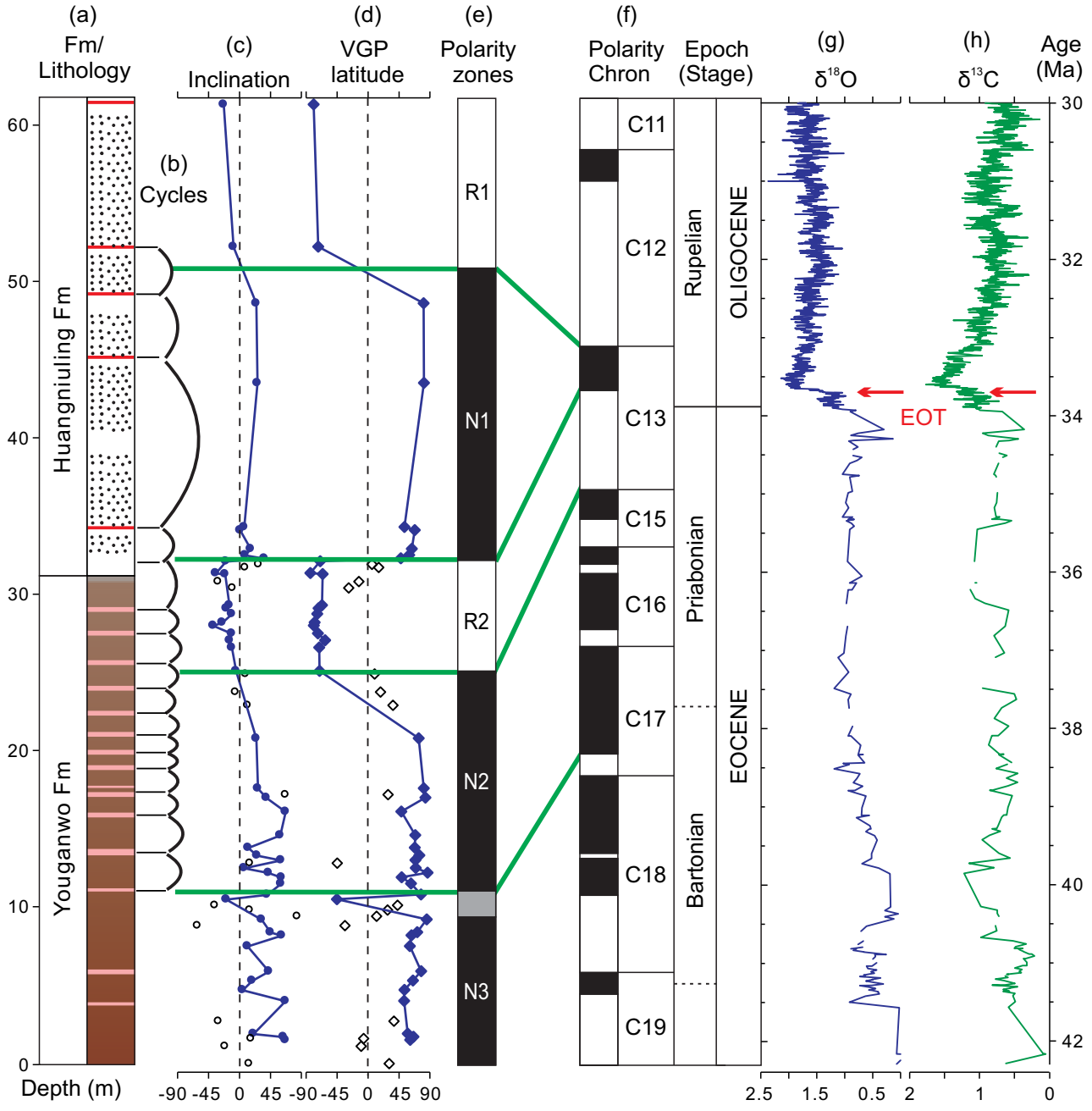
(a)
Fm/
Lithology
(b)
Cycles
(c)
Inclination
(d)
VGP
latitude
(e)
Polarity
zones
(f)
Polarity
Chron
Epoch
(Stage)
(g)
δ18O
(h)
δ13C
Age
(Ma)
Huangniuling Fm
Youganwo Fm
Depth (m)
R1
N1
R2
N2
N3
C11
C12
C13
C15
C16
C17
C18
C19
Rupelian
Priabonian
Bartonian
OLIGOCENE
EOCENE
EOT
-90 -45 0 45 -90 -45 0 45 90
2.5 1.5 0.5 2 1 0